J Mater Sci: Mater Electron (2015) 26:7415–7420
DOI 10.1007/s10854-015-3372-x

Fabrication of ZnO nanorods/Fe_3O_4 quantum dots nanocomposites and their solar light photocatalytic performance

Donglai Han[1,2,3] · Jian Cao[3] · Shuo Yang[1,2,3] · Jinghai Yang[3] · Bingji Wang[3] · Qianyu Liu[3] · Tingting Wang[3] · Haifeng Niu[3]

Received: 12 March 2015 / Accepted: 16 June 2015 / Published online: 25 June 2015

Abstract ZnO nanorods (NRs)/Fe_3O_4 quantum dots (QDs) nanocomposites were successfully synthesized via an easy electrostatic self-assembly method. The results showed that Fe_3O_4 QDs with an average diameter of 4–5 nm were well dispersed on the surface of the ZnO NRs with an average diameter of 118 nm, forming ZnO NRs/Fe_3O_4 QDs nanocomposites. The ZnO NRs/Fe_3O_4 QDs nanocomposites were used as photocatalysts for the degradation of Rhodamine B under solar light irradiation. The kinetic rate constant of the ZnO NRs/Fe_3O_4 QDs nanocomposites was two times higher than that of the ZnO NRs. The enhanced photocatalytic property was attributed to the extended absorption spectrum of the nanocomposites.

✉ Donglai Han
DLHan_1015@163.com

Jian Cao
caojian_928@163.com

Jinghai Yang
jhyang@jlnu.edu.cn

[1] Changchun Institute of Optics, Fine Mechanics and Physics, Chinese Academy of Sciences, Changchun 130033, People's Republic of China

[2] University of Chinese Academy of Sciences, Beijing 100049, People's Republic of China

[3] Key Laboratory of Functional Materials Physics and Chemistry of the Ministry of Education, Jilin Normal University, Siping 136000, People's Republic of China

1 Introduction

In the past decades, semiconductor photocatalysts have attracted considerable attention because of their promising potential for the conversion of solar into chemical energy, such as photocatalytic water splitting, photocatalytic degradation organic contaminants, toxic elimination of heavy metal ions etc. [1–3]. Among various semiconductor materials, ZnO are well-known direct band gap II–VI semiconductors, which have been studied intensively as good photocatalysts because of the rapid generation of electron–hole pairs by photo-excitation and the highly negative reduction potentials of the excited electrons [4–8]. However, ZnO has no visible-light response due to its large band gap of 3.37 eV [9]. Recently, much research has been focused on the development of visible-light-responsive photocatalysts to take advantage of the solar light resources more effectively because visible light constitutes a larger proportion than UV light in solar light [10–12]. To extend the application of photocatalyst, ZnO nanorods (NRs)/Fe_3O_4 quantum dots (QDs) nanocomposites have been extensively investigated because of their proven potential use as the next-generation building blocks for photocatalysis due to the special morphology and the efficient absorption in the visible region [13, 14]. However, the synthetic procedure of nanocomposites is rather complex and time-consuming [15, 16].

In this paper, we firstly prepared ZnO NRs which were grown on indium tin oxides (ITO) substrate through chemical bath deposition (CBD) method and then prepared Fe_3O_4 QDs through an improved chemical co-precipitation method. Finally we used a simple and environmental friendly electrostatic self-assembly method for fabricating ZnO NRs/Fe_3O_4 QDs nanocomposites, and their photocatalytic degradation of Rhodamine B (RhB) under solar

light irradiation were investigated. The thioglycolic acid modified ZnO NRs were conjugated with the citric acid modified Fe_3O_4 QDs to form stable nanocomposites through the reaction between the hydroxyl groups on the surface of the QDs and the carboxyl groups modified on the surface of the NRs. It is expected that integration of 1D ZnO NRs and 0D Fe_3O_4 QDs could yield superior photocatalytic properties compared to ZnO NRs.

2 Experimental section

2.1 Materials

Zinc nitrate ($Zn(NO_3)_2{\cdot}6H_2O$), zinc acetate ($Zn(C_2H_3O_2)_2{\cdot}2H_2O$), methenamine ($C_6H_{12}N_4$), thioglycolic acid (MPA), ferric chloride ($FeCl_3{\cdot}6H_2O$), ferrous chloride ($FeCl_2{\cdot}4H_2O$), PEG-4000, ethylene glycol, concentrated ammonia aqueous solution (25 %), citric acid and ethanol were all analytical grade (Shanghai Chemical Reagents Co.), and used without further purification.

2.2 Preparation and chemical modification of ZnO NRs

ZnO NRs were grown on indium tin oxides (ITO) substrate by chemical bath deposition (CBD) method, which can be found in our previous work [17]. Briefly, ITO substrates were firstly pretreated by coating the substrate with 5 mM of zinc acetate dehydrate ($Zn(C_2H_3O_2)_2{\cdot}2H_2O$) solution. Then, the aqueous solutions of 0.1 M zinc nitrate ($Zn(NO_3)_2{\cdot}6H_2O$) and 0.1 M methenamine ($C_6H_{12}N_4$) were mixed together to form solution A. The pretreated ITO substrates were immersed into solution A at 93 °C for 6 h to get ZnO NRs. ZnO NRs was modified by spinning MPA on the surface of the prepared ZnO NRs.

2.3 Preparation and chemical modification of Fe_3O_4 QDs

Fe_3O_4 QDs were prepared through an improved chemical co-precipitation method. $FeCl_3{\cdot}6H_2O$ (6 mmol), $FeCl_2{\cdot}4H_2O$ (10 mmol) and PEG-4000 (10 g) were dissolved in absolute ethylene glycol (250 ml). After stirring for 30 min at room temperature, 100 ml of concentrated ammonia aqueous solution (25 %) was added rapidly to the resulting complex. Then the reaction mixture was heated at 110 °C for 2 h under mechanical stirring, producing a black and homogeneous suspension. After cooling to room temperature, the precipitate was separated with a permanent magnet and washed with deionized water and ethanol for several times until the pH decreased to 7.0, followed by drying in a vacuum oven at 40 °C for 48 h.

Fe_3O_4 QDs was modified with citric acid as follows: 0.023 g of Fe_3O_4 QDs and 0.023 g of citric acid were dispersed in 250 ml of deionized water under mechanical stirring for 1 h to form the Fe_3O_4 water solution.

2.4 Preparation of ZnO NRs/Fe_3O_4 QDs nanocomposites

The prepared Fe_3O_4 water solution was spun on the surface of ZnO NRs, followed by drying at 200 °C for 60 s and then cooled down to room temperature. The above described operation was repeated 5 times.

2.5 Characterization of products

X-ray diffraction (XRD) pattern was collected on a MAC Science MXP-18 X-ray diffractometer using a Cu target radiation source. Scanning electron microscopy (SEM) pictures were collected on a Hitachi S-570. Transmission electron micrographs (TEM) and high-resolution transmission electron microscopy (HRTEM) images were taken on JEM-2100 electron microscope. UV–Vis absorption spectra were measured on an UV-5800 PC spectrometer.

2.6 Photocatalytic activity measurement

The photocatalytic activity measurements were as follows: the reaction system that containing RhB aqueous solutions and the as-synthesized ZnO NRs/Fe_3O_4 QDs nanocomposites were stirred thoroughly in the dark until reaching the adsorption equilibrium of the RhB before exposure to solar light irradiation. At a given irradiation time intervals, 4 ml of the solution were taken out. The degraded solutions were analyzed using the UV–Vis spectrophotometer (UV-5800 PC) and the characteristic absorption peak of the RhB solution was monitored. The degradation efficiency of the photocatalyst can be defined as follows [18]:

$$\text{Degradation}\,(\%) = (1 - C/C_0) \times 100\,\%$$

where C_0 is the initial concentration of RhB and C is the residual concentration of RhB at different illumination intervals.

The photodegradation of RhB follows pseudo-first-order kinetics, which can be expressed as follows [18]:

$$\ln(C/C_0) = kt$$

where k (min^{-1}) is the degradation rate constant.

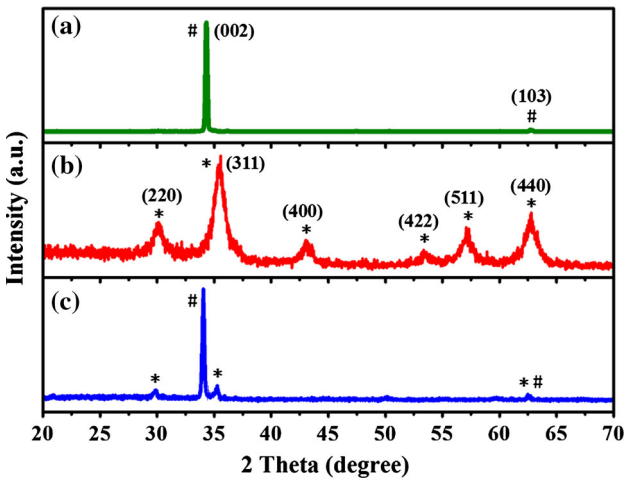

Fig. 1 XRD patterns of (*a*) ZnO NRs; (*b*) Fe_3O_4 QDs; (*c*) ZnO NRs/Fe_3O_4 QDs nanocomposites

3 Results and discussion

Figure 1 shows the XRD patterns of the ZnO NRs, Fe_3O_4 QDs and ZnO NRs/Fe_3O_4 QDs nanocomposites. As seen from Fig. 1a, all the diffraction peaks can be indexed as the wurtzite ZnO structure, which is consistent with the standard card (JCPDS No. 80-0074). It is noticeable that the (002) diffraction peak is stronger and narrower than the other peaks, suggesting a preferential growth direction along the c-axis [19]. Figure 1b displays the XRD pattern of Fe_3O_4 QDs. It can be seen that all the diffraction peaks can be indexed as the face-centered cubic structure, which is consistent with the standard card (JCPDS No. 19-0629). The average size estimated from the FWHM using the Debye–Scherrer formula [20] is about 5 nm, which is further demonstrated below by TEM studies. The XRD pattern of the ZnO NRs/Fe_3O_4 QDs nanocomposites (Fig. 1c) shows the characteristic peak of the ZnO NRs and Fe_3O_4 QDs, indicating the formation of the nanocomposites.

To further prove the formation of ZnO NRs/Fe_3O_4 QDs nanocomposites, we perform the SEM and HRTEM measurements to characterize the morphology of the samples. Figure 2a shows the SEM image of the ZnO NRs. It can be seen that the large-scale, vertically aligned ZnO NRs with high density and smooth surface are uniformly grown on the surface of ITO substrate. And the average diameter of ZnO NRs is about 118 nm. Figure 2b displays the HRTEM image of the Fe_3O_4 QDs. It can be seen that these QDs are well crystallized and the average diameter of the QDs is about 4–5 nm, which is consistent with the XRD results. The lattice fringes with the *d* spacing of 0.25 nm can be assigned to the (311) plane of the cubic Fe_3O_4 QDs [21, 22]. Figure 2c, d display the SEM images of the ZnO NRs/Fe_3O_4 QDs nanocomposites. Compared with the ZnO NRs (average diameter is about 118 nm), the average diameter is increased (average diameter is about 123 nm), and its surface is not smooth, demonstrating that the Fe_3O_4 QDs exist on the surface of ZnO NRs.

Figure 3 shows the absorption spectrum of ZnO NRs and ZnO NRs/Fe_3O_4 QDs nanocomposites, respectively. The absorption curve is smooth and the absorption peak is obtained at 355 nm (3.49 eV) for ZnO NRs (Fig. 3a), which displays blue-shift compared to the bulk ZnO (3.37 eV), indicating the formation of nanomaterials [23]. For ZnO NRs/Fe_3O_4 QDs nanocomposites (Fig. 3b), a broad absorption band from 370 to 500 nm can be observed, which can also prove that ZnO NRs have been modified by Fe_3O_4 QDs. Consequently, the ZnO NRs/Fe_3O_4 QDs nanocomposites with the extended absorption spectrum would exhibit the excellent photocatalytic performance under solar light irradiation.

The photocatalytic activity of ZnO NRs and ZnO NRs/Fe_3O_4 QDs nanocomposites was evaluated by the degradation of organic dye RhB under solar light irradiation. Figure 4 shows the concentration changes of RhB (C/C_0) during photodegradation as a function of solar light irradiation time, where C_0 and C are its initial concentration and the concentration of RhB after solar light irradiation, respectively. After the 7 h of solar light irradiation, the ZnO NRs/Fe_3O_4 QDs nanocomposites show a remarkable enhancement in the photodegradation of RhB compared with the ZnO NRs (Fig. 4). Seen from the images in the inset figure of Fig. 4, almost all of the initial RhB dyes are decomposed by ZnO NRs/Fe_3O_4 QDs nanocomposites, however, a great mass of RhB still remain in the solution of ZnO NRs.

The degradation kinetic of RhB under solar light irradiation was also investigated by plotting the relationship between $\ln(C_0/C)$ and irradiation time (Fig. 5). It can be seen that the curves of $\ln(C_0/C)$ versus irradiation time show linear lines, indicating a rather good correlation to first-order kinetics [24]. The determined k value for ZnO NRs and ZnO NRs/Fe_3O_4 QDs nanocomposites is 0.12 and 0.26 min^{-1}, respectively. The photocatalytic activity of ZnO NRs/Fe_3O_4 QDs nanocomposites is two times higher than that of ZnO NRs. Reusability is also important for the practical application of photocatalysts. The durability of the catalyst for the degradation of RhB under solar light irradiation was studied. Following a simple step of washing with water, the recycled photocatalyst was reused and the results of the photocatalyst degradation rate of RhB are shown in Fig. 5b. The ZnO NRs/Fe_3O_4 QDs nanocomposites does not exhibit a significant loss of activity after five cycles of the degradation reaction, which indicates the stable structure of the prepared nanocomposites throughout the photocatalytic process.

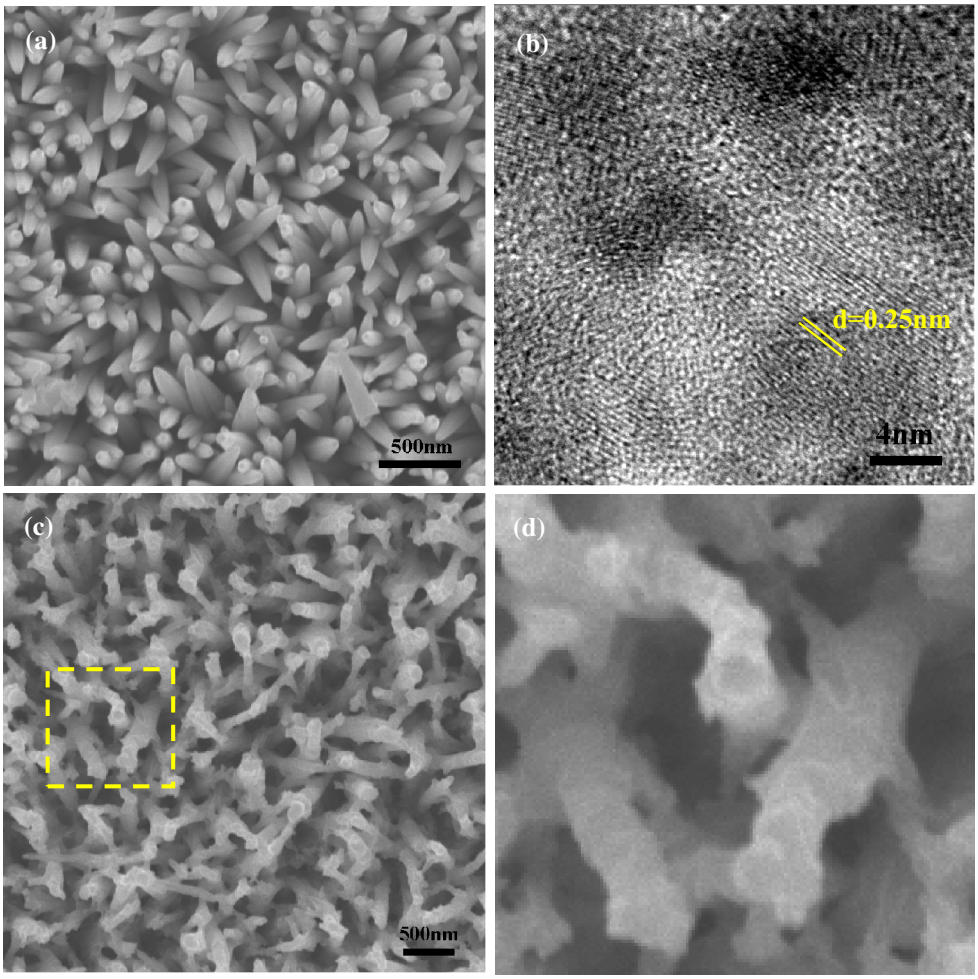

Fig. 2 **a** SEM image of ZnO NRs; **b** HRTEM image of Fe_3O_4 QDs; **c** SEM image of ZnO NRs/Fe_3O_4 QDs nanocomposites; **d** an enlarged view of the *yellow rectangle* in (**c**) (Color figure online)

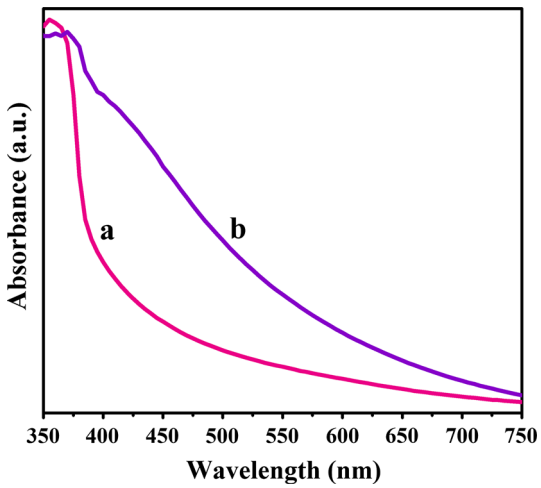

Fig. 3 UV–Vis absorption spectrum of (*a*) ZnO NRs and (*b*) ZnO NRs/Fe_3O_4 QDs nanocomposites

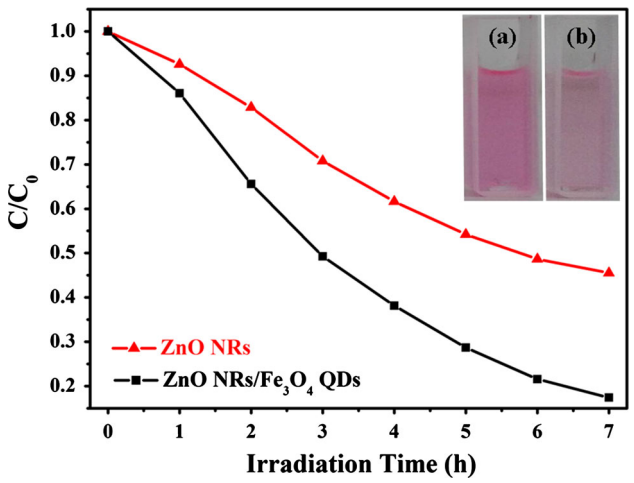

Fig. 4 Photocatalytic degradation of RhB under the irradiation of solar light with ZnO NRs and ZnO NRs/Fe_3O_4 QDs nanocomposites, the *inset figure* shows the image of the photocatalysis of RhB solution containing (*a*) ZnO NRs and (*b*) ZnO NRs/Fe_3O_4 QDs nanocomposites after the irradiation for 7 h

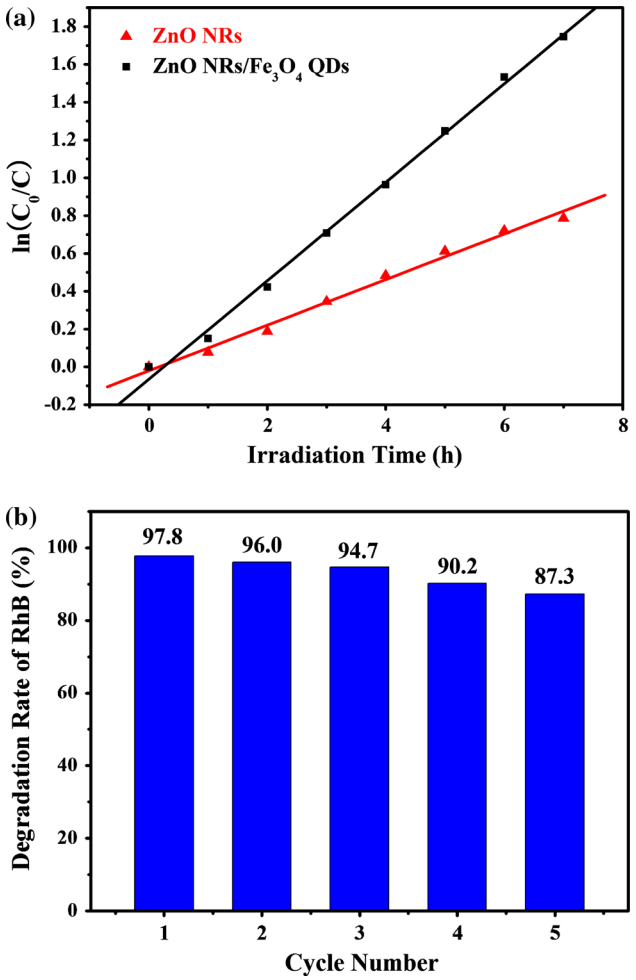

Fig. 5 **a** Plot of $\ln(C_0/C)$ as the function of solar light irradiation time for the photocatalysis of RhB solution containing ZnO NRs and ZnO NRs/Fe_3O_4 QDs nanocomposites; **b** the reusability of the ZnO NRs/Fe_3O_4 QDs nanocomposites under the solar light degradation of RhB solution

4 Conclusions

ZnO NRs/Fe_3O_4 QDs nanocomposites were successfully synthesized via electrostatic self-assembly method. The photocatalytic activity of ZnO NRs and ZnO NRs/Fe_3O_4 QDs nanocomposites was evaluated by the degradation of organic dye RhB under solar light irradiation. It was found that ZnO NRs/Fe_3O_4 QDs nanocomposites had higher photocatalytic activity and the kinetic rate constant of the ZnO NRs/Fe_3O_4 QDs nanocomposites was about two times higher than that of the ZnO NRs. Therefore, combining ZnO NRs and Fe_3O_4 QDs would open up a promising way to develop novel and highly efficient heterostructure photocatalysts.

Acknowledgments This work was financially supported by the National Programs for High Technology Research and Development of China (863) (Item No. 2013AA032202), the National Natural Science Foundation of China (Grant Nos. 61008051, 61178074, 11204104, 11254001).

References

1. R. Saravanan, M.M. Khan, V.K. Gupta, E. Mosquera, F. Gracia, V. Narayanan, A. Stephen, ZnO/Ag/CdO nanocomposite for visible light-induced photocatalytic degradation of industrial textile effluents. J. Colloid Interface Sci. **452**, 126–133 (2015)
2. M.M. Momeni, Y. Ghayeb, Visible light-driven photoelectrochemical water splitting on ZnO–TiO_2 heterogeneous nanotube photoanodes. J. Appl. Electrochem. **45**, 557–566 (2015)
3. C.M. Teh, A.R. Mohamed, Roles of titanium dioxide and ion-doped titanium dioxide on photocatalytic degradation of organic pollutants (phenolic compounds and dyes) in aqueous solutions: a review. J. Alloys Compd. **509**, 1648–1660 (2011)
4. F.A.L. Sánchez, A.S. Takimi, F.S. Rodembusch, C.P. Bergmann, Photocatalytic activity of nanoneedles, nanospheres, and polyhedral shaped ZnO powders in organic dye degradation processes. J. Alloys Compd. **572**, 68–73 (2013)
5. B.M. Rajbongshi, S.K. Samdarshi, B. Boro, W.K. Chan, H. Su, K.S. Wong, Multiphasic bi-component TiO_2–ZnO nanocomposite: synthesis, characterization and investigation of photocatalytic activity under different wavelengths of light irradiation. J. Mater. Sci. Mater. Electron. **26**, 377–384 (2015)
6. Y. Du, R.Z. Chen, J.F. Yao, H.T. Wang, Facile fabrication of porous ZnO by thermal treatment of zeolitic imidazolate framework-8 and its photocatalytic activity. J. Alloys Compd. **551**, 125–130 (2013)
7. Z.S. Li, Z.G. Liu, B.L. Li, D.H. Li, Y.P. Fang, Low-loading platinum decorated aligned ZnO nanorods and their photocatalytic and electrocatalytic applications. J. Mater. Sci. Mater. Electron. **26**, 3909–3915 (2015)
8. K.J. Liu, J.Y. Zhang, H. Gao, T.F. Xie, D.J. Wang, Photocatalytic property of ZnO microrods modified by Cu_2O nanocrystals. J. Alloys Compd. **552**, 299–303 (2013)
9. M. Villani, T. Rimoldi, D. Calestani, L. Lazzarini, V. Chiesi, F. Casoli, F. Albertini, A. Zappettini, Composite multifunctional nanostructures based on ZnO tetrapods and superparamagnetic Fe_3O_4 nanoparticles. Nanotechnology **24**, 135601–135610 (2013)
10. C.H. Cao, L. Xiao, C.H. Chen, Q.H. Cao, Magnetically separable Cu_2O/chitosan–Fe_3O_4 nanocomposites: preparation, characterization and visible-light photocatalytic performance. Appl. Surf. Sci. **333**, 110–118 (2015)
11. J. Jing, Y. Zhang, W. Li, W.W. Yu, Visible light driven photodegradation of quinoline over TiO_2/graphene oxide nanocomposites. J. Catal. **316**, 174–181 (2014)
12. Z. Wang, X. Liu, W. Li, H. Wang, H. Li, Enhancing the photocatalytic degradation of salicylic acid by using molecular imprinted S-doped TiO_2 under simulated solar light. Ceram. Int. **40**, 8863–8867 (2014)
13. C. Karunakaran, I. JebaSingh, P. Vinayagamoorthy, J. Jayabharathi, Magnetically separable CdS-deposited Fe_3O_4-implanted ZnO microrods for solar photocatalysis. Micro Nano Lett. **9**, 529–531 (2014)
14. M.S. Gohari, A.H. Yangjeh, Facile preparation of Fe_3O_4@AgBr–ZnO nanocomposites as novel magnetically separable visible-light-driven photocatalysts. Ceram. Int. **41**, 1467–1476 (2015)
15. X.H. Feng, H.J. Guo, K. Patel, H. Zhou, X. Lou, High performance, recoverable Fe_3O_4–ZnO nanoparticles for enhanced photocatalytic degradation of phenol. Chem. Eng. J. **244**, 327–334 (2014)

16. H.C. Su, J.Y. Dai, Y.F. Liao, Y.H. Wu, J.C.A. Huang, C.H. Lee, The preparation of Zn-ferrite epitaxial thin film from epitaxial Fe_3O_4:ZnO multilayers by ion beam sputtering deposition. Thin Solid Films **518**, 7275–7278 (2010)
17. Q.X. Zhao, L.L. Yang, M. Willander, B.E. Sernelius, P.O. Holtz, Surface recombination in ZnO nanorods grown by chemical bath deposition. J. Appl. Phys. **104**, 073526–073532 (2008)
18. S. Khanchandin, S. Kundu, A. Patra, A.K. Ganguli, Band gap tuning of ZnO/In_2S_3 core/shell nanorod arrays for enhanced visible-light-driven photocatalysis. J. Phys. Chem. C **117**, 5558–5567 (2013)
19. Y.F. Sun, J.H. Yang, L.L. Yang, M. Gao, X.N. Shan, Z.Q. Zhang, M.B. Wei, Y. Liu, L.H. Fei, H. Song, Less contribute ion of nonradiative recombination in ZnO nails compared with rods. J. Lumin. **134**, 35–41 (2013)
20. B.M. Manohara, H. Nagabhushana, D.V. Sunitha, K. Thyagarajan, B.D. Prasad, S.C. Sharma, B.M. Nagabhushana, R.P.S. Chakradhar, Synthesis and luminescent properties of Tb^{3+} activated cadmium silicate nanophosphor. J. Alloys Compd. **592**, 319–327 (2014)
21. X. Yu, J. Wan, Y. Shan, K. Chen, X. Han, A facile approach to fabrication of bifunctional magnetic-optical Fe_3O_4@ZnS microspheres. Chem. Mater. **21**, 4892–4898 (2009)
22. J. Su, M. Cao, L. Ren, C. Hu, Fe_3O_4 graphene nanocomposites with improved lithium storage and magnetism properties. J. Phys. Chem. C **115**, 14469–14477 (2011)
23. J.Y. Lao, J.Y. Huang, D.Z. Wang, Z.F. Ren, ZnO nanobridges and nanonails. Nano Lett. **3**, 235–238 (2003)
24. L. Jia, D.H. Wang, Y.X. Huang, A.W. Xu, H.Q. Yu, Highly durable N-doped graphene/CdS nanocomposites with enhanced photocatalytic hydrogen evolution from water under visible light irradiation. J. Phys. Chem. C **115**, 11466–11473 (2011)